IRAQI JOURNAL OF APPLIED PHYSICS LETTERS

The Iraqi Journal of Applied Physics Letters (IJAPLett) is a peer reviewed journal of high quality devoted to the publication of original research letters from applied physics and their broad range of applications. IJAPLett publishes quality original research letters in physics and its applications in the broadest sense. It is intended that the journal may act as an interdisciplinary forum for physics and its applications. Innovative applications and material that brings together diverse areas of physics are particularly welcome. IJAPLett aims to disseminate knowledge; provide a learned reference in the field; and establish channels of communication between academic and research experts, policy makers and executives in industry, commerce and investment institutions. IJAPLett is a quarterly specialized periodical dedicated to publishing original letters in: Alternative & Renewable Energy, Applied Mechanics & Thermodynamics, Applied Optics & Optical Design, Biophysics & Bioengineering, Cryptography & Applications, Electromagnetic Fields, Electronic Materials & Devices, Energy Generation & Conversion, Fluids Physics & Mechanics, Imaging, Microscopy & Spectroscopy, Laser Physics & Applications, Magnetism & Applications, Instrumentation, Measurements & Metrology, Nanostructures & Applications, Nonlinear & Ultrafast Optics, Nuclear Physics & Engineering, Optical Communications & Systems, Optoelectronics Devices & Applications, Organic Materials, Devices & Applications, Physical Chemistry & Biochemistry, Plasma, Discharge Physics & Applications, Quantum Physics & Spectroscopy, RF & Digital Communications, Semiconductors & Devices, Simulation & Modeling Research, Solar Energy & Devices, Solid State Physics & Applications, Structure & Properties of Matter, Superconductivity & Related Devices, Surfaces, Interfaces & Films, Thin Films & Applications, and Vacuum Science & Technology.

ISSN (Print)
1999-656X
ISSN (Online)
2958-6488

EDITORIAL BOARD

Editorial Office:
P. O. Box 88052, Baghdad 12631, IRAQ
Website: www.iraqiphysicsjournal.com
Emails: editor@iraqiphysicsjournal.com, editor_ijap@yahoo.co.uk, ijaplett.editor@gmail.com

ADVISORY BOARD

SPONSORED AND PUBLISHED BY
AMERICAN QUALITY FOR SCIENTIFIC PUBLISHING INC.
1479 South De Gaulle Ct, Aurora, CO 80018, United States

IRAQI JOURNAL OF APPLIED PHYSICS LETTERS

ISSN (Print): 1999-656X, ISSN (Online): 2958-6488

INSTRUCTIONS TO AUTHORS

CONTRIBUTIONS

Contributions to be published in this journal should be original research works, i.e., those not already published or submitted for publication elsewhere, individual papers or letters to editor.
Manuscripts should be submitted to the editor at the mailing address:

Iraqi Journal of Applied Physics Letters, Editorial Board, P. O. Box 88052, Baghdad 12631, IRAQ
Website: www.iraqiphysicsjournal.com
Email: editor@iraqiphysicsjournal.com, editor_ijap@yahoo.co.uk, ijaplett.editor@gmail.com

MANUSCRIPTS

Two hard copies with soft Word copy on a CD or DVD should be submitted to Editor in the following configuration:

- **One-column** Double-spaced one-side A4 size with 2.5 cm margins of all sides
- Times New Roman font (16pt bold for title, 14pt bold for names, 12pt bold for headings, 12pt regular for text)
- Manuscripts presented in English only are accepted.
- English abstract not exceed 100 words
- 4 keywords (at least) should be maintained on (PACS preferred)
- Author(s) should express all quantities in SI units
- Equations should be written in equation form (*italic* and symbolic) NOT in plain text
- Tables and Figures should be separated from text and placed in new pages after the references
- Charts should be indicated by the software used for generating them (e.g., Excel, MATLAB, Grapher, etc.)
- Figures and diagrams can be submitted in original colored forms for assessment and they will be returned to authors after provide printable copies
- Only original or high-resolution scanner photos are accepted
- For electronic submission, articles should be formatted with MS-Word software.

AUTHOR NAMES AND AFFILIATIONS

It is IJAPLett policy that all those who have participated significantly in the technical aspects of a paper be recognized as co-authors or cited in the acknowledgments. In the case of a paper with more than one author, correspondence concerning the paper will be sent to the first author unless staff is advised otherwise.
Author name should consist of first name, middle initial, last name. The author affiliation should consist of the following, as applicable, in the order noted:
- Company or college (with department name or company division), Postal address, City, Governorate or State, zip code, Country name, contacting telephone number, and e-mail

REFERENCES

The references should be brought at the end of the article, and numbered in the order of their appearance in the paper. The reference list should be cited in accordance with the following examples:
[1] X. Ning, R. Benford and M.R. Lovell, "On the Sliding Friction Characteristics of Unidirectional Continuous FRP Composites", *J. Tribol. Func. Mater.*, 124(1) (2002) 5-13.
[2] M. Barnes, "Stresses in Solenoids", *J. Appl. Phys.*, 48(5) (2001) 2000–2008.
[3] J. Jones, **"Contact Mechanics"**, Cambridge University Press (Cambridge, UK) (2000), Ch.6, p.56.
[4] Y. Lee, S.A. Korpela and R. Horne, "Structure of Multi-Cellular Natural Convection in a Tall Vertical Annulus", Proceedings of 7th International Heat Transfer Conference, U. Grigul et al., eds., Hemisphere (Washington DC), 2 (1982) 221–226.
[5] M. Hashish, "Waterjet Technology Development", High Pressure Technology, PVP-Vol. 406 (2000) 135-140.
[6] D.W. Watson, "Thermodynamic Analysis", ASME Paper No. 97-GT-288 (1997).
[7] C.Y. Tung, "Evaporative Heat Transfer in the Contact Line of a Mixture", Ph.D. thesis, Rensselaer Polytechnic Institute, Troy, NY (1982).

PROOFS

Authors will receive proofs of papers and are requested to return one corrected copy as a WORD file on a compact disc (CD) or by email. New materials inserted in the original text without Editor's permission may cause rejection of paper unless the handling editor is informed.

COPYRIGHT FORM

Author(s) will be asked to sign the IJAPLett Copyright Form and hence transfer copyrights of the article to the Journal soon after acceptance of it. This will ensure the widest possible dissemination of information.

OFFPRINTS

Authors will receive electronic offprint free of charge and any additional reprints can be ordered.

SUBSCRIPTION AND ORDERS

Annual fees (4 issues per year) of subscription are:
50 US$ for individuals inside Iraq; **200** US$ for institutions inside Iraq;
100 US$ for individuals abroad; **300** US$ for institutions abroad.

Effect of Silver Colloidal Concentration on Morphology of Silver Nanostructures Prepared by Chemical Reduction Method

Tabarak A. Al-Mashhadani, Firas J. Al-Maliki

Department of Physics, College of Science, University of Baghdad, Baghdad, IRAQ

Abstract

In this work, the effect of concentration of silver colloidal solution on the morphology of silver nanoparticles prepared from these solutions by chemical reduction method was studied. Different concentrations of silver colloidal solutions were prepared ($2x10^{-3}$, $3x10^{-3}$, $4x10^{-3}$ and $5x10^{-3}$ mol/L) and glass substrates were coated with the prepared samples using dip coating. The change in color of the prepared colloidal solutions was considered as a primary indication to the formation of nanoparticles within the solutions as well as the aggregation of the formed nanoparticles. Scanning electron microscopy was used to determine the range of particle size of the prepared silver nanostructures. It was found that the concentration is a primary tool to control the range of nanoparticle size in order to serve certain applications of precious metal nanoparticle such as silver.

Keywords: Nanoparticles; Chemical reduction; Silver nanoparticles; Concentration
Received: 7 November 2022; **Revised:** 11 December; **Accepted:** 18 December; **Published:** 1 January 2023

1. Introduction

Silver nanoparticles (Ag NPs) exhibit unique electrical, optical and magnetic properties when compared to the bulk silver. These properties make them excellent candidate for a wide range of applications [1,2]. Chemical reduction is the most frequently employed method for the preparation of Ag NPs as stable, colloidal dispersions in water or organic solvents [3]. In the aqueous solution, silver reduction occurs and nano-sized colloidal silver ions are produced [4]. The stability of any colloidal dispersion is of paramount importance and can be achieved by confining silver nanoparticles in a sol-gel matrix [5].

Nobel metal nanoparticles show brilliant colors due to the surface plasmon resonance absorption [6]. The examination of the surface plasmon resonance absorption is part of a large ongoing research field to investigate properties on the nanometer scale [7]. The color of metal nanoparticles depends on the shape and size of the nanoparticles and dielectric constant of the surrounding medium, leading to many studies on their synthesis and applications [8].

The bottom-up method of wet chemical nanoparticle preparation is based on reducing metal salts, electrochemical pathways or controlled decomposition of metastable organometallic compounds [9]. Chemical reduction methods to produce silver and gold nanoparticles vary in the choice of silver precursor or gold precursor, the reducing agent and their relative quantities and concentrations, the temperature, mixing rate, duration of reaction, etc [10]. Using different reagents and conditions for the synthesis large variations in the particle shape, size and size distributions may be expected. As for the source of silver, several salts are applicable [11], but silver nitrate is by far the most adopted for fabricating silver nanoparticles from silver salts, with the conditions for the synthesis.

The stronger reducing agents lead to produce smaller nuclei in the "seed" [12]. However, it is possible to obtain comparable reaction rates and particle sizes by adjusting the temperatures for the reactions. This will lead to differences in the crystal structure and thus the degree of crystallinity [13].

2. Experimental Part

Synthesis of silver nanoparticles in this work is based on a wet chemical method. The synthesis starting point is producing a silver nitrate ($AgNO_3$) solution. When $AgNO_3$ is dissolved in a suitable solvent, it splits into a positive silver ion (Ag^+) and a negative nitrate ion (NO^{-3}). In order to turn the silver ions into solid silver, the ions have to be reduced by receiving an electron from a donator. The following reactions illustrate the reduction of Ag^+ in a solution of ethanol

$$Ag^+_{(eq)} + e^- \rightarrow Ag_{(s)}$$

$$2Ag^+_{(eq)} + C_2H_5OH + H_2O \rightarrow 2Ag_{(s)} + C_2H_5O_2^- + 3H^+$$

After the silver germ is formed, it starts to grow and continue the growth until the equilibrium between the final nanoparticles and the Ag^+ of the solution is reached [14].

There are a number of parameters that can be adjusted in order to control the growth of particles. For example, small particles can be achieved by using a fast reduction agent such as $NaBH_4$. A fast reduction agent results in the formation of many silver germs at the beginning of the synthesis process. This high amount of silver germs will shorten the time required by the germs to grow and prevent the formation of large nanoparticles. If the solution is homogenous, the particles end up within a narrow size distribution [15].

The silver (Ag) colloids were prepared with different concentrations ($2x10^{-3}$, $3x10^{-3}$, $4x10^{-3}$ and $5x10^{-3}$ mol/L) as follows. A 50 mL starting solution of each concentration was prepared and a 25mL of silver nitrate ($AgNO_3$) solution was added to 100mL H_2O. On the other hand, a solution of 1% sodium citrate (0.5g in 50mL H_2O) was prepared and then a 125mL solution of $AgNO_3$ was heated up to boiling at 97°C. At a moment of boiling, 2.5 mL of 1% sodium citrate solution was added drop by drop as soon as boiling commences. Heating continues until the color of the solution changed to (pale yellow), as shown in Fig. (1). Then, the solution was removed from the heating source and left on stirrer to cool down to the room temperature.

The mechanism of the preparation reaction could be expressed as follows [16]:

$$4Ag+C_6H_5O_7Na_3+2H_2O \rightarrow 4Ag^0+C_6H_5O_7H_3+ 3Na+H+O_2\uparrow$$

In order to study the effect of reduction time, the experiment was repeated for 3, 5, 7, 9, 11, 15, 20 and 25 minutes after boiling point. The samples prepared after 9 minutes were considered as the optimum.

Drop casting method was used for coating of glass substrates with the prepared colloidal silver nanoparticles in order to perform the characterization tests on them.

Field-emission scanning electron microscopy (FE-SEM) was carried out on the prepared samples using an Inspect F50 FE-SEM instrument in order to introduce the effect of Ag colloid concentration on the minimum particle size of the produced Ag nanostructures.

3. Results and Discussion

It is clear from Fig. (2) that the color of the colloidal solution is gradually changed from light yellow to dark yellow, and finally becomes dark brown. This change in color confirms the formation and growth of silver nanoparticles with different particle size up to the aggregation. It is worth mentioning that the yellow color of silver nanoparticles is attributed to the surface plasmon resonance of these nanoparticles in this region of electromagnetic spectrum [17,18]. This change in color is also related to the addition of sodium citrate to the $AgNO_3$ solution.

Fig. (1) Photographs of the optimum samples prepared after 9 minutes reduction time with different concentrations of Ag colloids (left to right: $2x10^{-3}$, $3x10^{-3}$, $4x10^{-3}$ and $5x10^{-3}$ mol/L)

The precious metal nanoparticles (such as Ag) are very important for many spectroscopic, medical and biomedical applications as they provide exceptional features based on their structure as precious metals and on their sizes as nanostructures.

Figure (2) shows the FE-SEM images of the silver nanoparticles prepared in this work. From the first sight to these images, a uniform distribution of silver nanoparticles as nanospheres can be seen with particle size ranging within 15-66 nm. By looking carefully to these images, it is possible to note that the distribution of the nanoparticles is regular when the concentration is low as the particle size distribution gradually changes from small to large aggregations. For more explanation, the range of particle size will be discussed for each sample individually. In case of $2x10^{-3}$ mol/L concentration, the particle size is ranging within 33.20-47.17 nm with uniform distribution (Fig. 2a). In case of $3x10^{-3}$ mol/L concentration, the particle size is ranging within 14.86-65.94 nm (Fig. 2b). In case of $4x10^{-3}$ mol/L, the particle size is ranging within 26.43-54.00 nm with a semi-regular arrangement (Fig. 2c). Finally, in case of $5x10^{-3}$ mol/L, the particle size is ranging within 32.17-46.29 nm (Fig. 2d). These results give an indication that at a short reduction time, the particle size is smaller than the case of long reduction time. As well, the particle size might be estimated from the color of silver colloidal sample as the light yellow is a result of smaller particle size, while the dark yellow is a result of larger particle size. Changing to brown color may be an indication to increasing probability of aggregation through the colloidal solution.

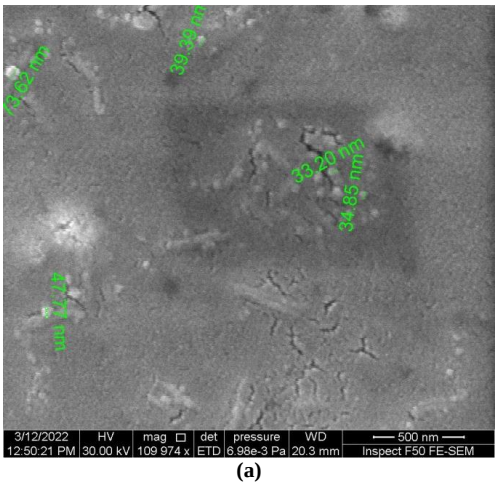

(a)

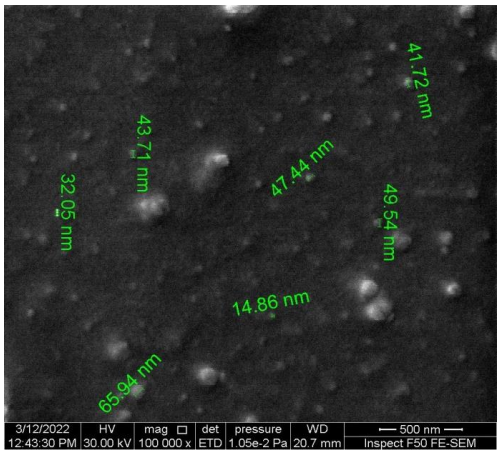

(b)

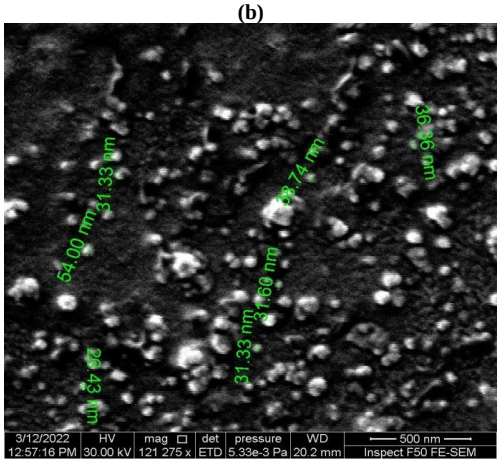

(c)

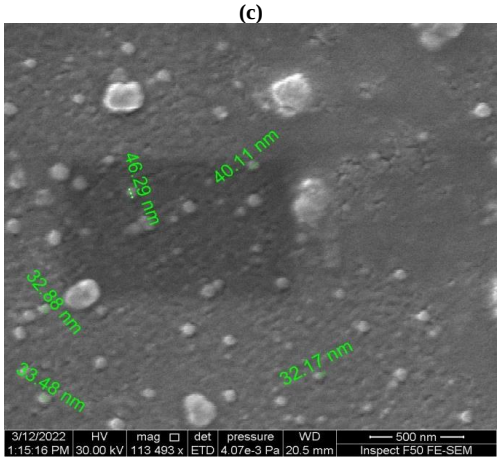

(d)

Fig. (2) Images of FE-SEM of the samples prepared after 9 minutes reduction time with different concentrations of Ag colloids (a) $2x10^{-3}$, (b) $3x10^{-3}$, (c) $4x10^{-3}$ and (d) $5x10^{-3}$ mol/L

4. Conclusion

In this work, the effect of concentration of silver colloidal solution on the morphology of silver nanoparticles prepared from these solutions by chemical reduction method was studied. The change in color of the prepared colloidal solutions gives an indication to the formation of nanoparticles within the solutions as well as the aggregation of the formed nanoparticles. The concentration of

silver colloidal solution is a primary tool to control the range of nanoparticle size in order to serve certain applications of precious metal nanoparticle such as silver.

References

[1] I. Khan, K. Saeed and I. Khan, "Nanoparticles: Properties, applications and toxicities", Arab. J. Chem., 12(7) (2019) 908-931.
[2] C. Caro et al., "Silver nanoparticles: sensing and imaging applications", INTECH, 65(51) (2010) 202-224.
[3] B.T. Chiad et al., "Study the optimum conditions of synthesis Ag NPs by chemical reduction method", J. Kerbala Univ., 11(4) (2013) 40-46.
[4] C. Gomez et al., "Medical Applications of Metallic Bismuth Nanoparticles", Pharmaceutics, 13(11) (2021) 1793.
[5] K.-C. Lee et al., "Size effect of Ag nanoparticles on surface plasmon resonance", Surf. Coat. Technol., 202 (2008) 5339-5342.
[6] A. Moores and F. Goettmann, "The plasmon band in noble metal nanoparticles: an introduction to theory and applications", New J. Chem., 30(8) (2006) 1121-1132.
[7] A. Pyatenko, M. Yamaguchi and M. Suzuki, "Synthesis of Spherical Silver Nanoparticles with Controllable Sizes in Aqueous Solutions", J. Phys. Chem. C, 111(2) (2007) 7910-7917.
[8] K.M.M.A. El-nour, A. Al-warthan and R.A.A. Ammar, "Synthesis and application of silver nanoparticles", Arab. J. Chem., 3(3) (2010) 135-140.
[9] Q.H. Tran, V.Q. Nguyen and A. Le, "Silver nanoparticles: synthesis, properties, toxicology, applications and perspectives", Adv. Nat. Sci.: Nanosci. Nanotechnol., 4 (2013) 1-20.
[10] L. Mahmudin et al., "The effect of the concentration of the stabilizer in the formation of a silver nanoparticle on the phenomenon of Surface Plasmon Resonance (SPR) as an active material for biosensor", J. Phys.: Conf. Ser., (2021) 1763-12064.
[11] J. Natsuki, T. Natsuki and Y. Hashimoto, "A Review of Silver Nanoparticles: Synthesis Methods, Properties and Applications", Int. J. Mater. Sci. Appl., 4(5) (2015) 325-332.
[12] T.K. Nguyen et al., "Mechanisms of Nucleation and Growth of Nanoparticles in Solution", Chem. Rev., 114(15) (2014) 7610-7630.
[13] N. Baig, I. Kammakakam and W. Falath, "Nanomaterials: a review of synthesis methods, properties, recent progress, and challenges", Mater. Adv., 2 (2021) 1821-1871.
[14] M. Zahoor et al., "A Review on Silver Nanoparticles: Classification, Various Methods of Synthesis, and Their Potential Roles in Biomedical Applications and Water Treatment", Water, 13(16) (2021) 2216.
[15] A. Syafiuddin et al., "A Review of Silver Nanoparticles: Research Trends, Global Consumption, Synthesis, Properties, and Future Challenges", J. Chin. Chem. Soc., 64 (2017) 732-756.
[16] M.Z. Hossain et al., "Synthesis of Spherical Silver Nanoparticles by Chemical Reduction Method", J. Bangladesh Chem. Soc., 30(20) (2021) 42-47.
[17] L. Mahmudin et al., "The effect of the concentration of the stabilizer in the formation of a silver nanoparticle on the Resonance (SPR) as an active material for biosensor", J. Phys.: Conf. Ser. (2021) 1763-012064.
[18] J. Fang, C. Zhong and R. Mu, "The Study of Deposited Silver Particulate Films by Simple Method for Efficient SERS", Chem. Phys. Lett., 401 (2005) 271-275.

Optical Microscopy of Highly-Pure Metal Oxide Nanoparticles Irradiated with Electromagnetic Radiation in Nonmetallic Hosts

Asraa M. Hameed, Mohammed A. Hameed

(1) Department of Physics, College of Science, University of Baghdad, Baghdad, IRAQ

Abstract

In this work, highly pure metal oxide nanoparticles (CuO, NiO, and TiO_2) were synthesized by a dc reactive magnetron sputtering technique. Nanopowders were extracted from the prepared thin films using a freezing-assisted ultrasound extraction technique. Also, multilayer thin films from the three oxides were prepared and their nanopowders were extracted as well. The prepared nanopowders were embedded in a nonmetallic host media and then irradiated with two different electromagnetic waves (x-ray and microwave). Optical microscopy was carried out on the prepared samples before and after irradiation with electromagnetic waves. Results showed that the prepared samples exhibit different responses to electromagnetic radiation that may be successfully employed in spectroscopic and marking applications.

Keywords: Nanoparticles; Reactive sputtering; Radiation-matter interaction; Marking

Received: 6 September 2022; **Revised:** 10 October; **Accepted:** 17 October 2022; **Published:** 1 January 2023

1. Introduction

Nanoparticles are a class of materials with properties distinctively different from their bulk and molecular counterparts [1,2]. Nanoparticles have unique optical properties that depend on their size and shape [3]. Excitation of such particles has a huge practical interest for fabrication of different media based on the properties and characteristics of such nanostructures and nanoparticles with unique optical properties and devices based on them [4,5]. As the properties of materials change as their size come close to the nanoscale, the nanoparticle size is similar to that of most biological molecules and structures. This makes them an interesting candidate for application in biomedical research [6]. The final destination of nanoparticles released in the environment is determined by their mobility in the different media (i.e., soil, water, air, etc.) as well as by their potential to biodegrade or undergo chemical transformation [7].

Nanotechnology can be used for various biomedical applications such as pharmaceutical excipients and drug delivery [8,9], cancer treatment and *in vivo* cytotoxicity [10], stable isotope tracing [11], bio-labeling and biosensors [12], medical imaging [13], artificial organs [14], and disinfection and sterilization [15].

Nanoparticles are used in biomedical applications as they offer many advantages to larger particles such as increased surface-to-volume ratio and enhanced properties [16]. Their high surface area to volume ratio can allow increased loading of therapeutics and such properties makes nanoparticles desirable for diagnostic and therapeutic applications [17]. Because of inherent size advantages, they can be used to probe more difficult-to-reach regions [18]. In order to employ for various nano medicinal applications, nanomaterials should be subjected to suitable surface modifications, to enhance the solubility and stability of nanosized materials in media of different phase or density as well as to impart them with biological properties and functionalities [19].

2. Experimental Part

A homemade dc reactive magnetron sputtering system was used in this work. Three highly-pure Cu, Ni and Ti targets (99.99%) were sputtered in presence of oxygen to deposit CuO, NiO, TiO_2 and

multilayer thin films on glass substrates. The deposition chamber was initially evacuated down to 0.001 mbar and then filled with gas mixture of argon and oxygen with mixing ratio of 1:1. The pressure of gas mixture was about 0.15 mbar and the discharge current was 40 mA.

The optimum deposition time of thin films was 3 hours, and the multilayer structure was deposited at different deposition times as follows, first layer was CuO deposited after 1 hour, second layer was NiO after 1:30 hours and the last layer was TiO_2 after 2 hours. More details on the sputtering system and its operation parameters can be found elsewhere [20]. The deposited thin films were extracted as powders by a technique known as conjunctional freezing-assisted ultrasonic extraction method [21,22].

In order to perform the marking experiment, a small amount of highly-pure nanopowder (CuO, NiO, TiO_2 and multilayer sample) was placed on a clean glass substrate, and then covered with a thin layer of rubber silicone. The substrate was then placed on a plate heater until the rubber silicone melted and the nanopowder sufficiently diffuse through the molten. It was then left to cool and solidify to form bulk sample, as shown in Fig. (1).

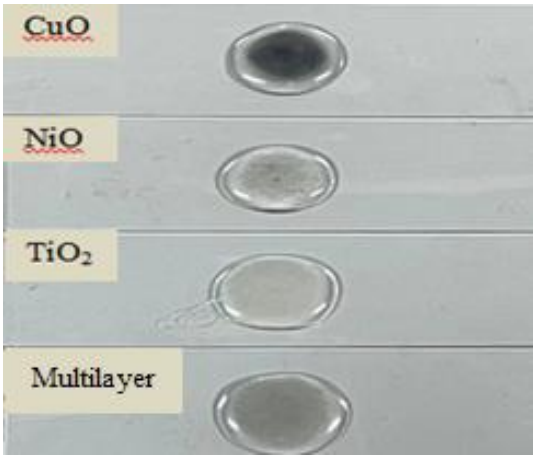

Fig. (1) Embedment of nanoparticles on silicone

The prepared samples (nanopowders in rubber silicone) were irradiated with two different electromagnetic waves; the first is x-ray using a GE Silhouette VR Rad Room instrument, with voltage was (40kV) and mass was (1mAs). The second is microwaves using a Morphy Richards AM925EF instrument, with power of 1400-1450W. The exposure time in both cases was 30 s.

The optical microscopy images of the samples were taken before and after irradiation using a XSZ-N107T optical microscope connected to a MC500 digital camera and personal computer. The dimensions (width and depth) of the samples were determined by the optical microscope at magnification power of 160/0.17.

3. Results and Discussion

Figure (2) shows the pictures of samples copper oxide (CuO), nickel oxide (NiO), titanium dioxide (TiO_2), and multilayer structure (M), were taken by optical microscopy before and after irradiation by x-rays for 30s. Pictures of samples were taken by optical microscopy for same dimensions (width and depth) and power of magnification (160/0.17) for all samples. A clear response of the nanoparticles was observed to electromagnetic radiation (X-ray). Because metal, and metal oxide has a high ability to absorb the energy of X-ray, but its presence inside the silicone host leads to the absorption of part of the X-ray energy by silicone, and thus the silicone heats up and becomes more transparent. So, the nanoparticles became clearer.

Figure (3) shows the pictures of samples before and after irradiation with Microwave for 30s, copper oxide (CuO), nickel oxide (NiO), titanium dioxide (TiO_2), and multilayer structure(M), were taken by optical microscopy at same dimensions (width and depth) and power of magnification (160/0.17) for all samples. A clear response of the nanoparticles was observed to electromagnetic radiation (microwave). Because nanoparticle (metal, and metal oxide) has ability to absorb the energy of Microwave, and convert it into vibrational energy. So, the aggregations has separated and became more organized.

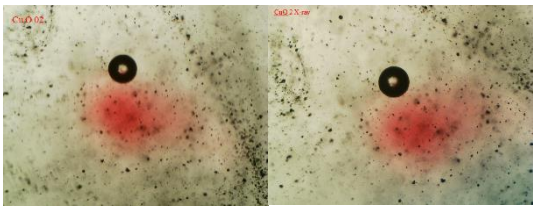

(a) CuO

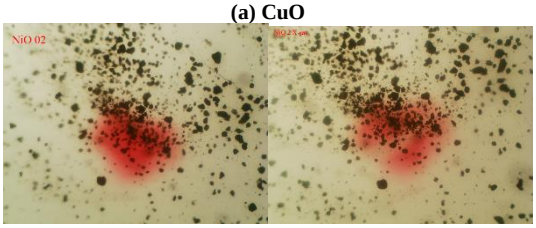

(b) NiO

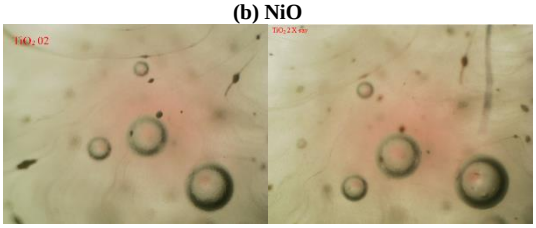

(c) TiO_2

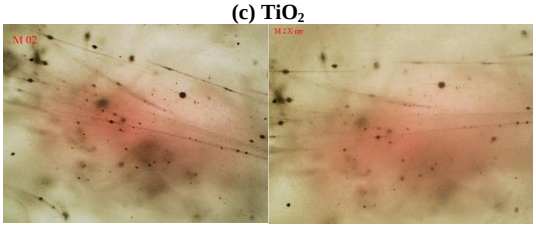

(d) Multilayer sample

Fig. (2) Microscopic images of prepared samples before (left) and after (right) irradiated with electromagnetic waves (x-ray) (a) CuO (b) NiO (c) TiO_2 (d) multilayer sample

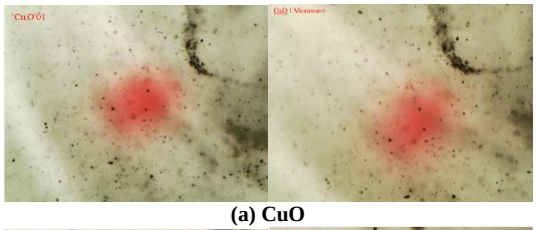

(a) CuO

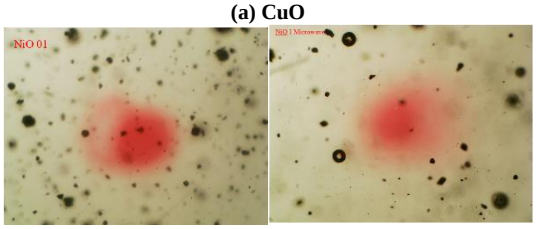

(b) NiO

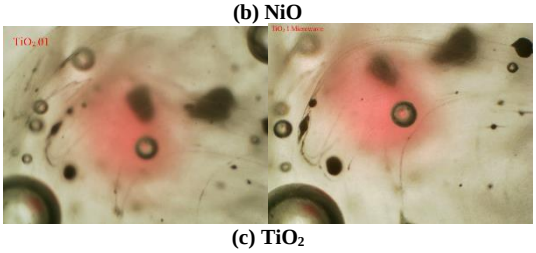

(c) TiO_2

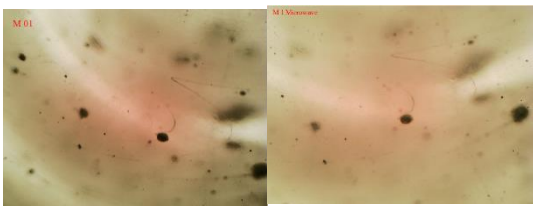

(d) Multilayer sample

Fig. (3) Microscopic images of prepared samples before (left) and after (right) irradiated with electromagnetic waves (microwaves) (a) CuO (b) NiO (c) TiO_2 (d) multilayer sample

1. Conclusion

In concluding remarks, High structural purity of the metal oxide samples as well as the multilayer samples was confirmed as no traces for other materials or compounds found in the final samples. This is attributed to the advantages of the DC reactive magnetron sputtering system used in this work. The multilayer samples can be used for tracing and marking applications as they show responsible fluorescence when excited by different wavelengths, especially the green light that represents the central region of electromagnetic spectrum. The prepared nanoparticles show sufficient response to the irradiation with X-ray and Microwaves as confirmed by the microscopic characterization. This response can be successfully for environmental and biomedical applications.

References

[1] Mohanraj, V. J., and Y. Chen. "Nanoparticles-a review." *Tropical journal of pharmaceutical research* 5.1 (2006): 561-573.

[2] Biswas, Pratim, and Chang-Yu Wu. "Nanoparticles and the environment." *Journal of the air & waste management association* 55.6 (2005): 708-746.

[3] Krasochko, P. A., et al. "Spectroscopic characteristics of colloidal solutions of metal nanoparticles." *Veterinaria I Kormlenie* (2021).

[4] Shaganov, Igor I., et al. "Influence of intermolecular interactions on spectroscopic characteristics of metal nanoparticles and their composites." *Physical Chemistry Chemical Physics* 16.44 (2014): 24536-24548.

[5] B.K. Nasser and M.A. Hameed, "Structural Characteristics of Silicon Nitride Nanostructures Synthesized by DC Reactive Magnetron Sputtering", Iraqi J. Appl. Phys., 15(4) (2019) 33-36.

[6] Manyasree, D., Kiran Mayi Peddi, and R. Ravikumar. "CuO nanoparticles: synthesis, characterization and their bactericidal efficacy." *Int J Appl Pharmaceut* 9.6 (2017): 71-74.

[7] Hristozov, Danail, and Ineke Malsch. "Hazards and risks of engineered nanoparticles for the environment and human health." *Sustainability* 1.4 (2009): 1161-1194.
[8] McNamara, Karrina, and Syed AM Tofail. "Nanoparticles in biomedical applications." *Advances in Physics: X* 2.1 (2017): 54-88.
[9] Thanh, Nguyen TK, and Luke AW Green. "Functionalisation of nanoparticles for biomedical applications." *Nano today* 5.3 (2010): 213-230.
[10] Biswas, Pratim, and Chang-Yu Wu. "Nanoparticles and the environment." *Journal of the air & waste management association* 55.6 (2005): 708-746.
[11] Saji, Viswanathan S., Han Cheol Choe, and Kelvin WK Yeung. "Nanotechnology in biomedical applications: a review." *International Journal of Nano and Biomaterials* 3.2 (2010): 119-139.
[12] Sung, Jean C., Brian L. Pulliam, and David A. Edwards. "Nanoparticles for drug delivery to the lungs." *Trends in biotechnology* 25.12 (2007): 563-570.
[13] Kim, S., Seong, K., Kim, O., Kim, S., Seo, H., Lee, M., ... & Lee, D. (2010). Polyoxalate nanoparticles as a biodegradable and biocompatible drug delivery vehicle. *Biomacromolecules*, *11*(3), 555-560.
[14] Huang, Yanyan, et al. "Emissive nanoparticles from pyridinium-substituted tetraphenylethylene salts: imaging and selective cytotoxicity towards cancer cells in vitro and in vivo by varying counter anions." *Chemical science* 7.12 (2016): 7013-7019.
[15] Gulson, Brian, et al. "Comparison of dermal absorption of zinc from different sunscreen formulations and differing UV exposure based on stable isotope tracing." *Science of the total environment* 420 (2012): 313-318.
[16] Hassan, Dilawar, et al. "Fluorescent Nanotechnology: An Evolution in Optical Sensors." *Current Analytical Chemistry* 18.2 (2022): 176-185.
[17] Niemirowicz, K., Markiewicz, K. H., Wilczewska, A. Z., & Car, H. (2012). Magnetic nanoparticles as new diagnostic tools in medicine. *Advances in medical sciences*, *57*(2), 196-207.
[18] El Shafie, Sarah Y., et al. "ANTIFUNGAL EFFECT OF PHOTOCATALYTIC NANO-TITANIUM DIOXIDE INCORPORATED IN SILICONE ELASTOMER." *Alexandria Dental Journal* 44.2 (2019): 52-60.
[19] Abiodun-Solanke, I. M. F., D. M. Ajayi, and A. O. Arigbede. "Nanotechnology and its application in dentistry." *Annals of medical and health sciences research* 4.3 (2014): 171-177.
[20] F.J. Al-Maliki and E.A. Al-Oubidy, "Effect of gas mixing ratio on structural characteristics of titanium dioxide nanostructures synthesized by DC reactive magnetron sputtering", Physica B: Cond. Matter, 555, 18-20 (2019).
[21] O.A. Hammadi, "Production of Nanopowders from Physical Vapor Deposited Films on Nonmetallic Substrates by Conjunctional FreezingAssisted Ultrasonic Extraction Method", Proc. ImechE, Part N, J. Nanomater. Nanoeng. Nanosys., 232(4) (2018) 135-140.
[22] O.A. Hammadi, "Effects of Extraction Parameters on Particle Size of Titanium Dioxide Nanopowders Prepared by Physical Vapor Deposition Technique", Plasmonics, 15 (2020) doi: 10.1007/s11468-020-01205-8.

FE-SEM and EDX Analysis of N-Doped TiO_2 and Co_3O_4 Nanostructures Prepared by DC Reactive Sputtering

Noor Alhuda H. Hashim, Firas J. Kadhim

Department of Physics, College of Science, University of Baghdad, Baghdad, IRAQ

Abstract

In this work, the field-emission scanning electron microscopy (FE-SEM) and energy-dispersive x-ray spectroscopy (EDX) were performed on the nitrogen-doped titanium dioxide (N-doped TiO_2) and cobalt oxide (Co_3O_4) nanostructures prepared by dc reactive magnetron sputtering technique. Results of the FE-SEM showed that the N-doped TiO_2 sample exhibits homogeneity of particle distributions and the minimum particle size was found 28.09 nm. As well, the Co_3O_4 sample contain spherical nanoparticles with minimum particle size of 37.32 nm. The EDX results showed that the weight percentages of Ti, O and N in the final N-doped TiO_2 sample were 49.1%, 40.7%, and 0.9%, respectively, which may confirm the role of nitrogen as dopant in the structure of TiO_2. Also, the EDX results showed that the elemental composition of the Co_3O_4 sample consist of 72.3% Co and 19.9% O_2, which is corresponding to the structural phase of Co_3O_4.

Keywords: Nanostructures; Reactive sputtering; Magnetron sputtering; Metal oxides; EDX
Received: 9 November 2022; **Revised:** 13 December; **Accepted:** 20 December; **Published:** 1 January 2023

1. Introduction

Electrochromic materials is the materials that change its color when an electric field is applied [1]. These materials can be either organic or inorganic materials [2], the organic materials suffer from leakage problems when they operated in their liquid phase [3], while the inorganic materials have a good electrochemical reversibility, chemical stability and high coloring efficiency where organic EC materials display poor durability [4]. There are two different types of EC materials which are classified in accordance with the coloration mechanisms [5,6]:

- Cathodic EC materials, which are coloring under ion insertion ''reduction process''
- Anodic EC materials, which are coloring under ion extraction ''oxidation process''

Most non-metal elements such as B, C, N and F have also been used as dopants in TiO_2 photocatalysts [7-11]. Nitrogen-doped TiO_2 is by far the most intensively studied system among the other non-metal doped materials. The N atoms can be easily introduced to TiO_2 lattice due to their comparable atomic size to oxygen, small ionization energy and high stability [12]. TiO_2 doped with non-metal (N-atoms) at oxygen sites serve as charge (electrons and holes) trapping sites to reduce electron hole recombination rate .and allow absorption into the visible region due to the introduction of dopant impurity level in TiO_2 band gap. Thus, the photocatalytic performance is enhanced compared to undoped photocatalyst [13,14]. Titanium dioxide is doped with nitrogen could reduce the band gap of TiO_2 and improve its photocatalytic activity in the visible-light region [15,16]. Thus, can be used as photoelectrochromic layer of PECD.

Cobalt Oxide nanostructured have a wide range of applications due to their shape dependent activities and unique size , optical, magnetic, electronic, chemical, electrochemical , mechanical properties [17-19]. The preparation and characterization of cobalt oxides have been extensively studied due to attractive applications in batteries, solar cells, catalysis, corrosion protective coatings, magnetic nanostructures and magnetic storage systems, electrochromic. Cobalt oxide has been reported to be a good anodic coloration material for the EC application [20,21].

Transparent conducting oxide (TCO) layer is made of a transparent material with low resistivity deposited on a top of substrate. The main role of TCO is to conduct electrons to and out of the adjacent electrochromic layer. The sheet resistance should be less than 20 Ω/sq is needed with more than 85 % transmission in the visible region of the spectrum. The materials are typically tin-doped indium oxide (ITO), antimony-doped tin oxide or fluorine-doped tin oxide (FTO) and/or Aluminum doped Zinc oxide (Al-ZnO) deposited on glass or flexible substrate are used [22]. ITO is conductive and transparent for wavelengths near the UV-Visible region and acts as a transparent conducting electrode in PECD [23,24].

In this work, the field-emission scanning electron microscopy (FE-SEM) and energy-dispersive x-ray spectroscopy (EDX) were performed on the nitrogen-doped titanium dioxide (N-doped TiO_2) and cobalt oxide (Co_3O_4) nanostructures prepared by dc reactive magnetron sputtering technique for photoelectrochromic devices.

2. Experimental Part

A dc reactive magnetron sputtering system was use to prepare thin films of N-doped TiO_2 and Co_3O_4 on borosilicate substrates. Highly-pure titanium and cobalt sheets were used as targets to be sputtered. In order to prepare N-doped TiO_2 thin films, highly-pure nitrogen gas was mixed with the argon and oxygen in the gas mixtures with mixing ratio ($Ar:O_2:N_2$) of 76:19:5. This low content of nitrogen was appropriate to ensure the doping of titanium dioxide structures with nitrogen and not to form dominant titanium nitride. The operating parameters were inter-electrode distance of 4 cm, applied voltage of 2.5 kV, discharge current of 40 mA and deposition time of 3 hours. These parameters were the same used to prepare Co_3O_4 thin films but using $Ar:O_2$ gas mixture only with mixing ratio of 60:40.

The nanopowders were extracted from the thin film samples using the conjunctional freezing-assisted ultrasonic extraction method was employed to remove nanopowders from the deposited thin films. This process may be used to extract nanopowders from deposited thin films using PVD technologies. This technique is quick, low-cost, reliable, and extremely clean, making it ideal for large-scale samples [25].

Field-emission scanning electron microscopy (FE-SEM) was performed on the prepared samples as nanopowders using an Inspect F 50 FE-SEM instrument, which is integrated with a PHENOM PURE 30000X instrument to perform EDX spectroscopy on the prepared samples. This technique is used for imaging the nanostructures on the surface of the prepared sample and determining the elemental composition of these nanostructures.

3. Results and Discussion

The FE-SEM images of the N-doped TiO_2 and Co_3O_4 samples prepared in this work are shown in figures (1) and (2), respectively. The N-doped TiO_2 sample exhibits homogeneity of particle distributions, which is one of the most important advantages of dc magnetron sputtering technique used for synthesis of nanostructures. The inter-space between nanoparticles, which is an inevitable result to the presence of gas species (N) within the structure [24]. The minimum particle size was found 28.09 nm.

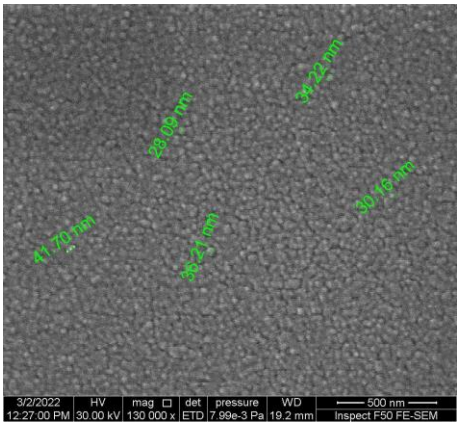

Fig. (1) FE-SEM image of N-doped TiO_2 thin film sample prepared in this work

The FE-SEM image in Fig. (2) shows that the Co_3O_4 nanoparticles are spherical with minimum particle size of 37.32 nm, and the aggregated particles indicating a good connectivity between these nanoparticles. The

nanoparticles can form complex assemblies referred as aggregates, which typically consist of particles in the nanoscale (5-50 nm). They are held together by weak forces arising from the van der Waals, van der Waals leads to an electrostatics effect through the residual charge of the structure. Ambient humidity plays an important role in determining the fundamental mechanical response and dynamics of these assemblies [26,27].

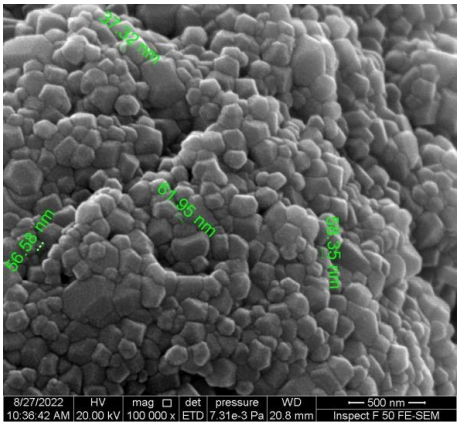

Fig. (2) FE-SEM image of Co_3O_4 thin film sample prepared in this work

The energy-dispersive x-ray (EDX) spectra of the prepared sample was recorded and analyzed as shown in figures (3) and (4). The summary of the elemental compositions of both samples are presented in the tables below these figures. The EDX spectrum in Fig. (3) revealed the presence of titanium, oxygen and nitrogen atoms in the final sample and thus the formation of N-doped TiO_2 thin films was confirmed. With the existence of Ti, O and N in the final sample, the weight ratio of Ti was found to be 49.1%, 40.7% for O and 0.9% for N. The 9.4% of carbon is resulted from handling the sample inside the instrument.

According to Fig. (4), the major peaks are for the Co and O forming the cobalt oxide sample, and the minor peak attributed to the C. The elemental composition of the cobalt oxide nanostructures shows 72.3% of cobalt, 19.9% of oxygen corresponding to the structural phase of Co_3O_4 and 7.8% of carbon. Using sputtering technique, the formation of nanostructures with required composition can be controlled by controlling the gas mixing ratio. Also, many metal oxides can be prepared by sputtering technique with good control of their compositions.

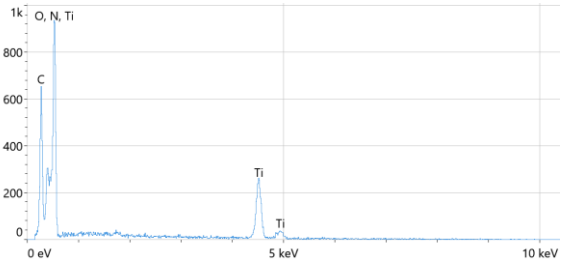

Element	Atomic %	Weight %	Weight % Error
C	17.7	9.4	0.2
N	1.4	0.9	0.4
O	57.7	40.7	1.0
Ti	23.2	49.1	1.2

Fig. (1) EDX spectrum of N-doped TiO_2 thin film sample prepared in this work

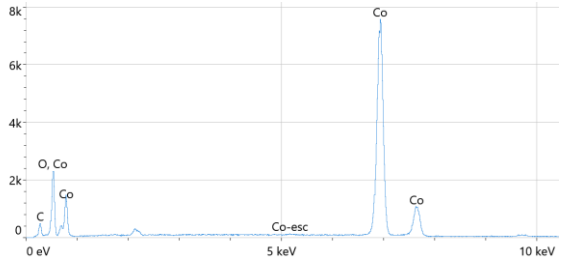

Element	Atomic %	Weight %	Weight % Error
C	20.8	7.8	0.2
O	39.9	19.9	0.2
Co	39.4	72.3	0.4

Fig. (2) EDX spectrum of Co_3O_4 thin film sample prepared in this work

4. Conclusion

In concluding remarks, highly-pure nanostructures of doped metal oxide (e.g., N-doped TiO_2 and undoped metal oxide (e.g., Co_3O_4) can be prepared using dc reactive magnetron sputtering technique. The specifications of the prepared nanostructures can be considered as high quality for some applications requiring high structural purity and uniform shape such as photoelectrochromic devices and smart windows. The preparation process presented in this work can be described as low-cost, highly reliable, and highly reproducible.

References

[1] I.P. Koziarskyi et al., "Optical Properties of Cobalt Oxide Thin Films", IEEE Int. Conf. on

Nanomaterials: Applications & Properties, (NAP-2020), Sumy, Ukraine, 9-13 Nov. 2020
[2] V. Patil et al., "Synthesis and Characterization of Co_3O_4 Thin Film", Sci. Res., 2(1) (2012) 1-7.
[3] H. Heli and H. Yadegari, "Nanoflakes of the cobaltous oxide, CoO: Synthesis and characterization", Electrochimica Acta, 55 (2010) 2139-2148.
[4] A.E. Kaloyeros et al., "Review–cobalt thin films: trends in processing technologies and emerging applications", ECS J. Solid State Sci. Technol., 8 (2019) 119.
[5] R. Drasovean, S. Condurache-Bota and N. Tigau, "Structural and Electrical Characterization of Cobalt Oxide Semiconductors", J. Sci. Arts, 13(2) (2010) 379-384.
[6] R. Hippler et al., "Deposition of cobalt oxide films by reactive pulsed magnetron sputtering", Surf. Coat. Technol., 405 (2021) 126590.
[7] M.K. Khalaf, F.J. Kadhim and O.A. Hammadi, "Effect of Adding Nitrogen to the Gas Mixture on Plasma Characteristics of a Closed-Field Unbalanced DC Magnetron Sputtering System", Iraqi J. Appl. Phys., 10(1) (2014) 27-31.
[8] M.A. Hameed and Z.M. Jabbar, "Preparation and Characterization of Silicon Dioxide Nanostructures by DC Reactive Closed-Field Unbalanced Magnetron Sputtering", Iraqi J. Appl. Phys., 12(4) (2016) 13-18.
[9] R. Hippler et al., "Characterization of a magnetron plasma for deposition of titanium oxide and titanium nitride films", Contrib. Plasma Phys., 45 (2005) 348-357.
[10] L.D. Kadam, S.H. Pawar and P.S. Patil, "Studies on ionic intercalation properties of cobalt oxide thin films prepared by spray pyrolysis technique", Mater. Chem. Phys., 68 (2001) 280-282.
[11] E.A. Al-Oubidy and F.J. Kadhim, "Effect of Gas Mixing Ratio on Energy Band Gap of Mixed-Phase Titanium Dioxide Nanostructures Prepared by Reactive Magnetron Sputtering Technique", Iraqi J. Appl. Phys., 14(4) (2018) 19-23.
[12] O.A. Hammadi, "Production of nanopowders from physical vapor deposited films on nonmetallic substrates by conjunctional freezing-assisted ultrasonic extraction method", Proc. IMech. Eng. Part N: J. Nanomater. Nanoeng. Nanosyst, 232(4) (2018) 135-140.
[13] O.A. Hammadi, "Conjunctional Freezing-Assisted Ultrasonic Extraction of Silicon Dioxide Nanopowders from Thin Films Prepared by Physical Vapor Deposition Technique", Iraqi J. Appl. Phys., 15(4) (2019) 23-28.
[14] O.A. Hammadi, "Effects of Extraction Parameters on Particle Size of Titanium Dioxide Nanopowders Prepared by Physical Vapor Deposition Technique", Plasmonics, 15(6) (2020) 1747-1754.
[15] H.E. Swnason et al., **"Standard X-Ray Diffraction Powder Patterns"**, International Center for Diffraction Data (ICDD) (Washington DC, 1971), NBS monograph 25, Sec. 9, p. 29
[16] X. Zhu et al., "Co_3O_4 nanoparticles with different morphologies for catalytic removal of ethyl acetate", Catal. Comm., 156 (2021) 106320.
[17] N.A.H. Hashim and F.J. Kadhim, "Structural and Optical Characteristics of Co_3O_4 Nanostructures Prepared by DC Reactive Magnetron Sputtering", Iraqi J. Appl. Phys., 18(4) (2022) 31-36.
[18] O.A. Hammadi and N.E. Naji, "Fabrication and Characterization of Polycrystalline Nickel Cobaltite Nanostructures Prepared by Plasma Sputtering as Gas Sensor", Phot. Sen., 8(1) (2018) 43-47.
[19] C. Suryanarayana, **"Mechanical Alloying and Milling"**, Marcel Dekker (NY, 2004), Ch. 7, p. 111.
[20] N. Francelosi et al., "Role of the reactive sputtering deposition power in the phase control of cobalt oxide films", Am. Vac. Soc., 36 (2018) 061512.
[21] S.C. Endres, L.C. Ciacch and L. Madler, "A review of contact force models between nanoparticles in agglomerates, aggregates and films", J. Aerosol Sci., 153 (2021) 105719.
[22] R. Lakra et al., "Synthesis and characterization of cobalt oxide (Co_3O_4) nanoparticles", Mater. Today: Proc., 2 September 2020.
[23] K. Maaz, **"Cobalt"**, InTech Open (Croatia, 2017), Ch. 4, p. 56.
[24] A.N. Naveen and S. Selladurai, "Investigation on physiochemical properties of Mn substituted spinel cobalt oxide for supercapacitor applications", Electrochimica Acta, 125 (2014) 404-414.
[25] S. Baset et al., "Size measurement of metal and semiconductor nanoparticles via UV-vis absorption spectra", Dig. J. Nanomater. Biostruct., 6(1) (2011) 1-8.
[26] R. Saravanan, **"Novel Ceramic Materials"**, Materials Research Forum LLC (Millersville PA, 2016), Vol. 2, Ch. 4, p. 49.
[27] M. Kumar Patel et al., "Reactive sputtering growth of Co_3O_4 thin films for all metal oxide device: a semitransparent and self-powered ultraviolet photodetector", Mater. Sci. Semicond. Process., 74 (2018) 74-79.

Employment of Laser-Induced Breakdown Spectroscopy for Elemental Composition Analysis in Dentistry

Asmaa N. Ahmed[1], Ali A. Hussain[2], Kadhim A. Aadim[2]

[1] Al-Hussain University College, Karbala, IRAQ
[2] Department of Physics, College of Science, University of Baghdad, Baghdad, IRAQ

Abstract
In this work, the laser-induced breakdown spectroscopy (LIBS) technique was used to introduce the elemental composition of tooth samples and hence evaluate the progressive growth as a diagnosis tool in dentistry. Results have shown the potential use of the LIBS technique for discriminating between wisdom teeth tissue of women's. The concentration matrix elements (Ca and Na) and non-matrix elements (other elements) increase in women's age group less than 30 year. This technique is highly reliable, flexible and appropriate for local treatment and diagnosis.

Keywords: Laser-induced breakdown spectroscopy; Biophysics; Dentistry; Laser applications
Received: 12 November 2022; **Revised:** 16 December; **Accepted:** 23 December; **Published:** 1 January 2023

1. Introduction

Light emitting plasmas have been studied in earnest since the 1920s, and laser induced plasmas since 1960 [1]. Laser Induced Breakdown Spectroscopy (LIBS) is basically an emission spectroscopy technique where atoms and ions are primarily formed in their excited states as a result of interaction between a tightly focused laser beam and the material sample. The interaction between matter and high density photons generates plasma plume, which evolves with time and may eventually acquire thermodynamic equilibrium [2]. LIBS has become of interest to many researchers owing to its unique properties such as minimal time duration of preparing the sample, low cost capability of being used in all three states of materials, and its nondestructive nature [3]. This method is used to detect corpse's bones and humans' fossils. It is also used to detect backgrounds characteristic like age and statues of bodies [4]. This method is used in dentistry to detect the caries parts of a tooth, and also in teeth modification. Spectral analysis plasma glow made by pulse laser can be used safely and accurately to monitor the occurrence of cancer [5-7]. Due to the increase use of lasers in clinical dental practice, LIBS can be achieved to create one-dimensional or two-dimensional concentrations maps as a function of location or depth which permits the study of elements distribution.

Teeth help you chew your food, making it easier to digest. Each type of tooth has a slightly different shape and performs a different job. Types of teeth include:

Incisors are the eight teeth in the front of your mouth (four on top and four on bottom). These are the teeth that you use to take bites of your food. Incisors are usually the first teeth to erupt at around 6 months for your baby teeth, and between ages 6 and 8 for your adult set.

Canines are the next type of teeth to develop. These are your sharpest teeth and are used for ripping and tearing food apart. Primary canines generally appear between 16 and 20 months, with the upper canines coming in just ahead of the lower canines. In permanent teeth, the order is reversed, with lower canines erupting around age 9 and the uppers arriving between ages 11 and 12.

Premolars are used for chewing and grinding food. Adults have four premolars on each side of their mouths — two on the upper

and two on the lower jaw. There are no primary premolars; the first premolars appear around age 10, with the second premolars arriving about a year later. These take the places of the first and second primary molars (described below).

Molars are also used for chewing and grinding food. Primary molars, also known as deciduous molars, appear between 12 and 28 months, and are replaced by the first and second premolars (four upper and four lower) described above.

Wisdom teeth, or third molars, are the final teeth to develop. Most of us have four wisdom teeth, one in each corner of the mouth. They usually emerge during our late teens or early twenties [9].

Often times, wisdom teeth become trapped or impacted in the jawbone or simply fail to erupt. This can cause crowding or displacement of other teeth or lead to the development of localized tooth decay, infection, or gum disease. Impacted wisdom teeth are set in the jawbone in unusual positions, sometimes horizontally, which stops them from erupting in a normal way.

Electron temperatures can be calculated using intensities of same species according to Boltzmann equation [10].

$$\ln\left(\frac{I_{ji}\lambda_{ji}}{A_{ji}g_j}\right) = -\frac{E_j}{kT_{exc}} + \ln\left(\frac{hc\,N_o}{4\pi\,U(T)}\right) \qquad (1)$$

where I_{ji} is the intensity of the spectral line of the transition from level j to i, λ_{ji} is the wavelength, A_{ji} is the transition probability, g_j is the statistical weight, E_j is the energy value of higher level, and T_{exc} is the excitation temperature. Thus, a plot of $\ln\left(\frac{I_{ji}\lambda_{ji}}{A_{ji}g_j}\right)$ versus the energy of the upper level E_j yields a straight line called Boltzmann plot, its slope is equals to $-(KT_{exc})^{-1}$.

According to the Saha-Boltzmann equation electron density can be deduced from the intensity ratio of two lines matching to different ionization stages [10, 11].

$$n_e = \frac{2(2\pi m_e kT)^{3/2}}{h^3}\,\frac{I^I_{mn}A_{jk}g^{II}_j}{I^{II}_{jk}A_{mn}g^I_m}\,e^{-(E_{ion}+E^{II}_j-E^I_m)/kT} \qquad (2)$$

where E_m and E_j are the upper level energies of neutral and single ionized transitions, E_{ion} is the ionization energy and n_e is the electron density.

2. Experimental Part

Samples of wisdom teeth were supplied by the dental clinics in Yarmouk Hospital (Baghdad, Iraq). They were washed in sodium hypochlorite diluted with distilled water for 15 min to remove contamination from the outer surface, dried at room temperature, and then they were preserved in formalin solution.

The optical emission spectra for plasma ablated near teeth samples surfaces were recorded using LIBS experimental system shown in Fig. 1. It consists of pulse Nd: YAG laser of 10 ns duration, 10 Hz pulse repetition frequency, using wavelength of 1064nm, with energy (400 mJ). The laser beam was focused on the surface of the sample which is located at the focal length of a converging lens (f=10 cm). Optical fiber adjusted at 45° with beams directed at 5 cm distance from the sample where plasma was generated. Spectroscopic information was obtained from the laser induced targets plasma spectra in air, under atmospheric pressure. Each spectrum was obtained over a 150-1000 nm wavelength range.

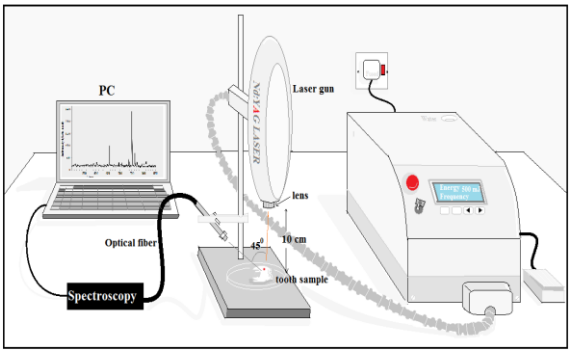

Fig. (1) The conventional LIBS system configuration

3. Results and Discussion

The results obtained from wisdom teeth for women's showed statistically significant differences for Ca, K, Na, Zn, Mg and Sr. Concentrations of Ca, K and Na were higher in females age group less than 30 year, while the atomic lines intensities of these elements decreased at age group above 30 year.

Figures (2) and (3) show LIBS spectra of wisdom teeth for women's in spectral range 150-1000 nm at energy of 400 mJ respectively.

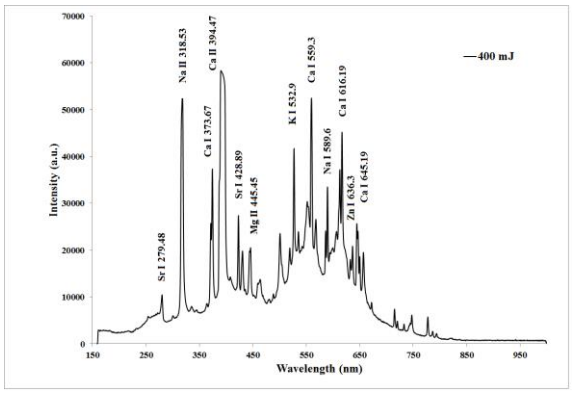

Fig. (2) LIBS spectrum of wisdom tooth for women's age group less than 30 year at 400mJ

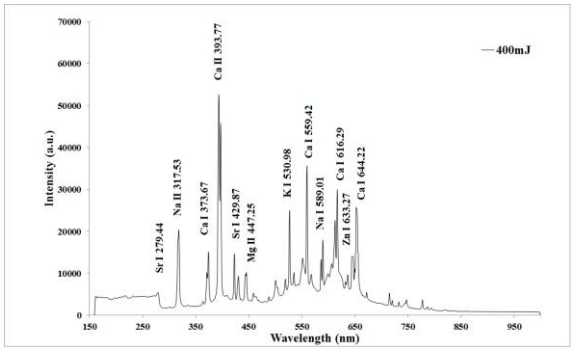

Fig. (3) LIBS spectrum of wisdom tooth for women's age group above 30 year at 400mJ

Also, these elements Ca, K, Na, Mg, Zn and Sr were detected in the wisdom teeth for women's at age group 40 year and above. Changes of the elements relative composition of teeth are different with age group.

Figures (4) and (5) show the LIBS spectra of wisdom teeth for women's at age groups 40 year and (above 40) respectively. It can be observed that the relative intensity of the elements Ca, K, Na and Zn are higher in women's age group 40 year than in women's age group above 40 year. Also a high content of Sr and Mg was detected in the wisdom teeth.

4. Conclusion

The results of the present work have shown the potential use of the LIBS technique for discriminating between wisdom teeth tissue of women's. The concentration matrix elements (Ca and Na) and non-matrix elements (other elements) increase in women's age group less than 30 year. Exploiting the changes in concentration ratios between the matrix elements (Ca and Na) and non-matrix elements (K, Zn, Mg and Sr), represented by the relative changes in the line intensities as seen in the LIBS spectra, of different ages. The concentration of several atomic elements in wisdom teeth samples decrease with age. Negative correlation for Ca and Na content in wisdom teeth samples with age was noticed. The Ca concentration increases in young women's compare with old woman's. Further developments could introduce LIBS allowing the dentist to monitor and control the problems of teeth during laser drilling of tooth.

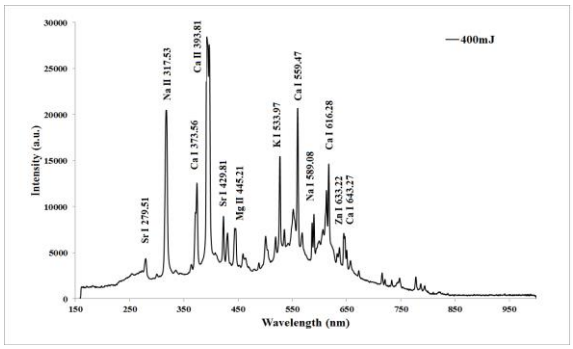

Fig. (4) LIBS spectrum of wisdom tooth for women age group 40 year at 400mJ

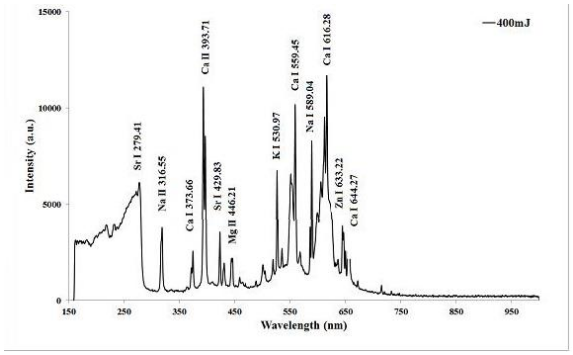

Fig. (5) LIBS spectrum of wisdom tooth for women's age group above 40 year at 400mJ

References

[1] L. Radziemski and D. Cremers, "A brief history of laser induced breakdown spectroscopy", *Spectrochim. Acta*, 87 (2013) 3-10.

[2] K. Song, Y. Lee and J. Sneddon, "Applications of laser induced breakdown spectrometry", *Appl. Spectro. Rev.*, 32(3) (1997) 183-235.
[3] D. Cremers and L. Radziemski, **"Handbook of Laser Induced Breakdown Spectroscopy"**, John Wiley & Sons, Ltd. (2006) ISBN: 0-470-09299-8.
[4] M. Martin et al., "High resolution applications of laser-induced breakdown spectroscopy for environmental and forensic applications", *Spectrochim. Acta Part B*, 62(12) (2007) 1426-1432.
[5] O. Samek et al., "Quantitative analysis of trace metal accumulation in teeth using laser-induced breakdown spectroscopy", *Appl. Phys. A*, 69(1) (1999) 179-182.
[6] O. Samek, H. Telle and D. Beddows, "Laser-induced breakdown spectroscopy: a tool for real-time, *in vitro* and *in vivo* identification of carious teeth", *BMC Oral Health*, 1(1) (2001) article 1.
[7] A. Kumar et al., "Characterization of malignant tissue cells by laser-induced breakdown spectroscopy", *Appl. Opt.*, 43(28) (2004) 5399-5403.
[8] O. Olea-Mejia et al., "Scanning Electron Microscopy and Energy Dispersive Spectroscopy microanalysis applied to human dental specimens under laser irradiation for caries prevention", *Microscopy: Adv. in Sci. Res. Edu.* (2014).
[9] P.F. Gonçalves et al., "Dental cementum reviewed: development, structure, composition, regeneration and potential functions", *Braz. J. Oral Sci.*, 4(12) (2005) 651-658.
[10] Tognoni E. et al., "A numerical study of expected accuracy and precision in calibration-free Laser-induced Breakdown Spectroscopy in the assumption of ideal analytical plasma", *Spectrochim. Acta Part B*, 62(12) (2007) 1287-1302.
[11] S.Z. Mortazavi et al., "Time-resolved evolution of metal plasma induced by Q-switched Nd:YAG and ArF-excimer lasers", *Opt. Laser Technol.*, 62 (2014) 32-39.
[12] J.D. Le May et al., **"Low-Density Microcellular Materials"**, MRS bulletin, Cambridge University Press (1990).
[13] T.J.M. Boyd and J.J. Sanderson, **"The Physics of Plasmas"**, Cambridge University Press (2003), ISBN: 0521459125, 9780521459129.

Electrical Characteristics of CuInSTe Thin Films Prepared by Quenching-Assisted Vacuum Coating Technique

Bushra A. Hasan

Department of Physics, College of Science, University of Baghdad, Baghdad, IRAQ

Abstract

In this work, the role of substrate temperature on the electrical characteristics of CuInSTe/CdS thin film heterojunctions was investigated. The frequency and temperature dependencies upon AC conductivity were investigated in the frequency range 100Hz-10MHz and temperature range of 303-453K. The AC activation energy was found to increase from 0.1132 to 0.1258 eV with increasing substrate temperature from 293 to 423K and to decrease to 0.0962 eV with increasing frequency from 100 to 10^7 Hz. The exponents show a nonsystematic sequence with the increment of substrate temperature. The obtained results gave indication that there is a relation between the structure and preparation temperature as well as heat treatment. The current-voltage characteristic of CuInSTe/CdS heterojunction under illumination shows that the CuInSTe/CdS produced at 423 K is the best one.

Keywords: CuInSeTe; Thin films; Quenching-assisted vacuum coating; Electrical characteristics
Received: 9 November 2022; **Revised:** 13 December; **Accepted:** 20 December; **Published:** 1 January 2023

1. Introduction

The quaternary compounds (CuInSeTe, CuInSeS and CuInSTe) are considered as absorbing materials for solar cell applications. There are few data available about their bulk material properties [1-3] as well as thin films [4,5-7]. The available data refer that there is a strong dependence between their structure and preparation conditions, which may be due to the amorphous nature as well as the dependencies of their properties on the ambient conditions. Solaiman has investigated the electrical properties [8] and optical properties [9] for CuInSTe, CuInSeTe and CuInSeS thin films.

The present paper is devoted to perform quaternary alloy of CuInSTe and then to prepare thin films at various substrate temperatures and point out the dependencies of dielectric properties on deposition condition using relation between the preparation temperature and these properties.

2. Experimental Part

The alloys of CuInSTe were prepared by quenching technique. The exact amount of high purity (99.999%) copper (Cu), indium (In), selenium (Se) and tellurium (Te) of about 99.9999% elements, in accordance with their percentages, are used. The mixed elements are sealed in evacuated (~10^{-3}torr) quartz ampoule (25cm in length and 8mm internal diameter). Ampoules containing the elements were heated up to 1273K and frequently rocked at the highest temperature for 10 hours. The quenching was done in water immediately after taking out the ampoules from the furnace. Edward vacuum coating system was used to deposit CuInSTe films at different substrate temperatures (303, 373 and 423K).

Aluminum electrodes with thickness of 200nm were deposited on each adjacent surfaces of specimen by thermal evaporation technique under pressure of 10^{-5} Torr using an Edward E306A coating unit. The specimen was fixed in a holder and placed into temperature-controlled oven (type Heresies electronic). High and low holder terminals are connected to dielectric analyzer (type Hewlett-Packard HP4274A & HP4275A), the third holder terminal was connected to the earth. The dielectric parameters like total resistance (R_T), total capacitance (C_T) and

dissipation factor (tanδ) were measured (in parallel mode) under certain frequency range 10^2-10^6 Hz. The AC conductivity (σ_{AC}) has been estimated from the obtained dielectric data using the following relation:

$$\varepsilon_2 = \sigma_{AC} / \varepsilon_o \quad (1)$$

where the dielectric constants (ε_1 and ε_2) can be calculated using the following relation:

$$\varepsilon_1 = C.t / \varepsilon_0 .A \quad (2)$$

where C is the capacitance, ε_0 is the permittivity of free space, t is film thickness, is the angular frequency, A is the effective area for capacitance, and AC is the AC conductivity given by:

$$\sigma_{AC} = \omega \varepsilon_0 \varepsilon_1 \tan\delta \quad (3)$$

where tanδ is the dielectric tangent loss

The conductivity measured with an AC technique is given by:

$$\sigma(\omega,T) = \sigma_{dc}(T) + a(T)\omega^S \quad (4)$$

The first term $\sigma_{dc}(T)$ in Eq. (5) is the direct current or DC conductivity, ω=0, conductivity, while the second term a(T) is the temperature-dependence factor and "s" is an exponent in the range 0<s<1. This equation estimates that if the first term is less than the second term, then $\sigma(\omega,T) \propto \omega^s$, so that the plot diagram of σ versus log(ω) is a straight line with slope s. While if the first term is larger than the second term (with increasing temperature), then the plot of σ versus ω in log scale should give a horizontal straight-line.The current-voltage measurements in the dark were done for the CuInSTe/CdS heterojunction using Keithley digital electrometer 616 and D.C. power supply .The bias voltage was varied in the range of -1 to 1V in the case of forward and reverse bias.

3. Results and Discussion

Figure (1) shows the angular frequency dependence of total conductivity $\sigma_{tot}(w)$ for CuInSTe films deposited at different substrate temperatures in the heat treatment range 303-453K. It is clear that there is proceeding increase of $\sigma_{tot}(\omega)$ that increased in the whole frequency range, i.e., the AC conductivity, and the dominated or, σ_{DC} conductivity is much lesser than the σ_{AC}, which indicates that the electronic polarization and the conductivity is purely AC.

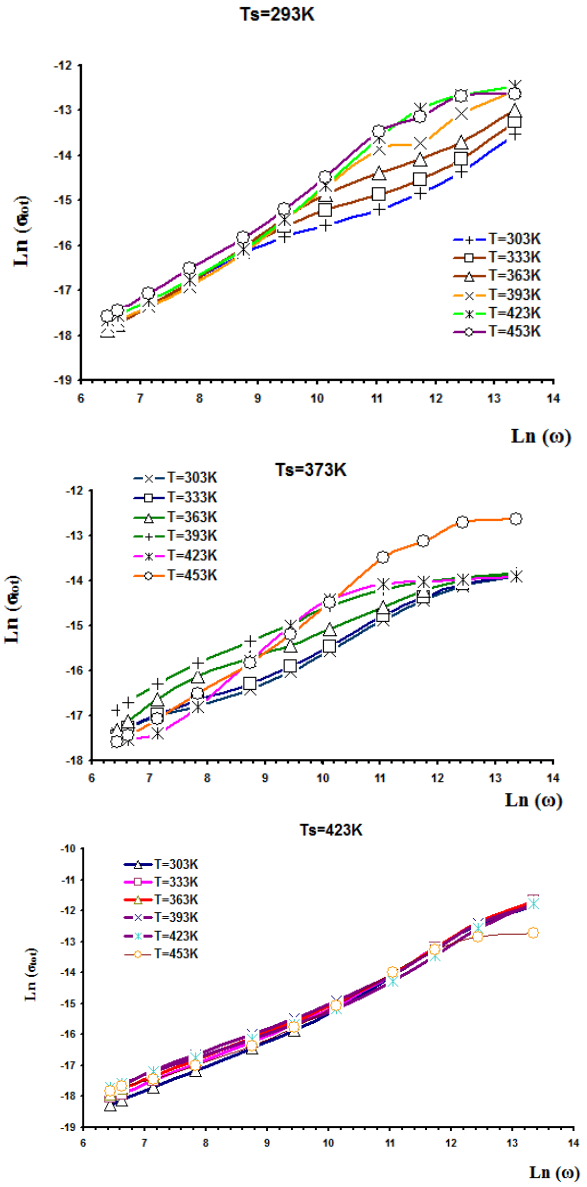

Fig. (4) Variation of Ln(σ_{tot}) with Ln(ω) for as deposited CuInSTe thin films and annealed at different temperatures

The exponent s, which is the slope of $dLn[\sigma_{tot}(\omega)]/d(\omega)$ decreases with increasing substrate temperature (T_S) in the low temperature range, while s increases at elevated temperatures, i.e., 423K, with increasing of T_S. The value of s increased with increasing heat treatment temperature of films deposited at T_S=373K. Also, s showed progress decreasing with oven temperature for samples deposited at 423K. Thus, the suitable models for these samples are SP and CBH, respectively.

The AC activation energy, E_{AC}, for CuInSTe films are estimated from the drawing of $Ln\sigma_{tot}(\omega)$ against the reciprocal absolute

temperature, as indicated in Fig. (2). The results show that each sample declared one E_{AC}. On the other side, there is a direct relation between E_{AC} and frequency, while there is an inverse relation between E_{AC} and T_S. The E_{AC} decreases from 0.1132 to 0.0962eV, while it increases from 0.1132 to 0.1258eV with increasing frequency from 1kHz to 100kHz as well as increasing substrate temperature from 293 to 423K, respectively. The increase in frequency results in an increase of vibrating energy and hence the E_{AC} values will be decreased. This indicated that conductivity is purely AC, while the elimination of the localized states and vacancies explained the increase of E_{AC} with increasing T_S. Seto's [10] proposed the presence of large amount of trapping states at the grain boundary that able to capture free charge carries. These charged states at grain boundary create potential barriers, which oppose the passage of carriers from grain to neighboring ones, where their sites increase with increasing T_S, which resulted in decreasing conductivity or increasing E_{AC} values.

Variation of current under illumination at different power density with biasing voltage of p-CuInSTe/n-CdS thickness of 700nm deposited at various temperatures (303, 373 and 423) K is plot in Fig. (3). It is obvious that photo current increases with basing voltage which reflect the rectifying properties i.e. the cell permit current to pass at forward biasing but there is no current at reverse biasing except the saturation current. The photocurrent increases exponentially for forward biasing , there take place due to due to high level injection of carriers such that the applied voltage is no longer totally developed across the depletion region while break down can occur at the high reverse biasing as a result of impact ionization or Zener tunneling. These mechanisms can be separated by temperature dependence.

It clear that increasing of depositing temperature had significant effect on the illumination current, i.e., there is valuable increment in the illumination current at elevate substrate temperature, this arise from the phase transformation from amorphous to crystalline structure, the illumination current of exhibit to increase with the increase of Ts as a result of increase of grain size values.

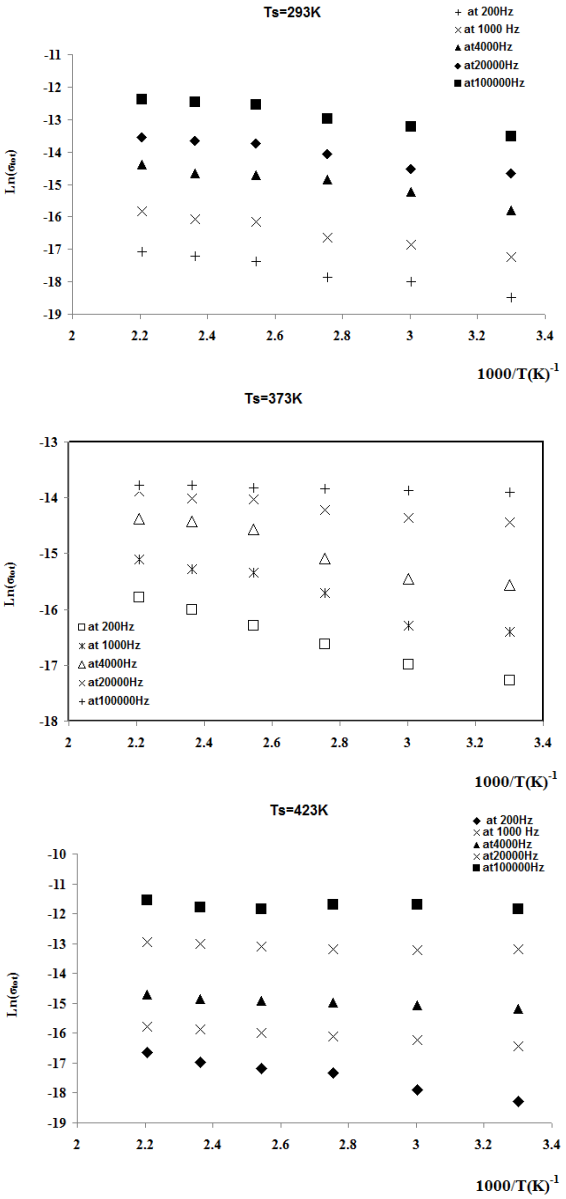

Fig. (2) Variation of Ln(σ_{tot}) with 1000/T for CuInSTe thin films deposited at different substrate temperatures

The V_{OC} tends to vary in nonsystematic sequence with T_S, i.e., V_{OC} increases and decreases with increasing T_S, and its increase resulted from decreasing of electron affinity χ between the CuInS and Te system and CdS layer, while the decreasing of V_{oc} ascribes to increasing of χ between the two layers of the junction. Anyway the high values V_{oc} and I_{sc} at T_S =423K for CuInSTe/CdS indicates that this junction at this condition of preparation is the most suitable for solar cell fabrication. For

photocurrent consideration which is equal to short circuit current $I_{sc,}$ the smaller band gap the better because mare photons are collected. It is found that maximum efficiency can be obtain when the band gap lie in the range (0.8-1.4eV). The ideal efficiency increases primarily due to the increasing of V_{oc} while the photocurrent is increased linearly with the intensity [11].

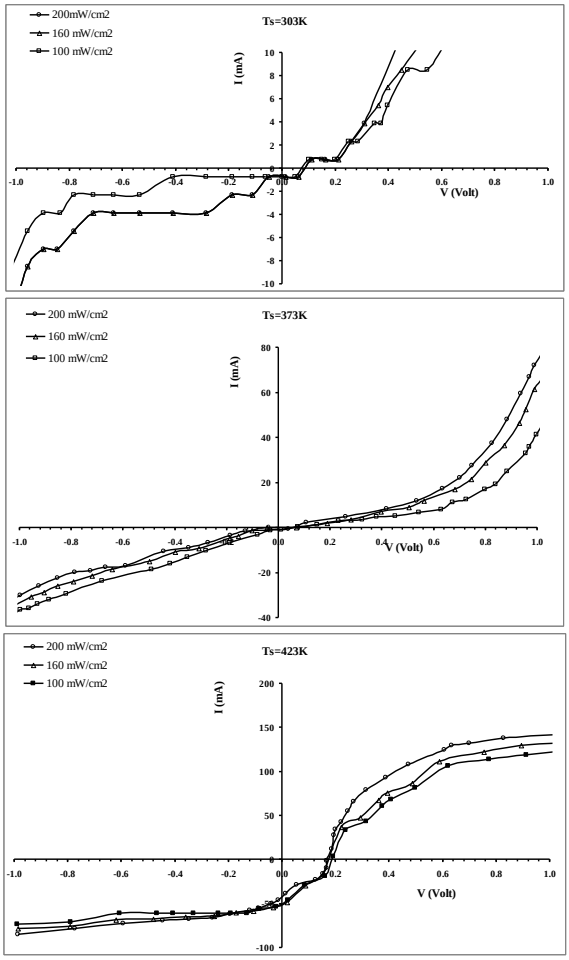

Fig. (3) I-V characteristics for p-CIS'T/n-CdS heterojunction with t=700nm at different substrate temperature and power density

4. Conclusion

From the results obtained from this work, it can be concluded that the as deposited CuInSTe thin films deposited at elevated temperature are type p-type. It is evident from the polarizability values that CuInSTe thin films can be used as resistor in electronic circuits.

References

[1] B.A. Hasan and D.A. Umran, "Dielectric permittivity and ac conductivity of CuInSeTe thin films", *Semicond. Sci. Technol.*, 27 (2012) 125014.

[2] B.A. Hasan, "AC Conductivity and dielectric analysis of CuInSSe Thin Films", *Int. J. Thin Film Sci. Tech.*, 2(1) (2013) 29-36.

[3] R. Diaz, M. Leon and F. Reuda, "Characterization of Cu–In–Se–Te system in thin films grown by thermal evaporation", *J. Vac. Sci. Technol. A*, 10 (1992) 295-300.

[4] K. Inakoshi et al., "Preparation of $CuIn(S_xSe_{1-x})_2$ thin films by sulfurization and Selenization", *Solar Energy Mater. Solar Cells*, 50(1) (1998) 37-42.

[5] K. Subbaramiah and V. Sundara Raja, "Structural and optical properties of spray-deposited $CuIn(S_{1-x}Se_x)_2$ thin films", *Thin Solid Films*, 208 (1992) 247-251.

[6] T. Ohashi et al., "$CuIn(S_xSe_{1-x})_2$ Thin Films by Sulfurization", *Japan J. Appl. Phys.*, 34 (1995) 4159-4166.

[7] S. Kuranouchi and T. Nakazawa, "Study of one-step electrodeposition condition for preparation of $Culn(Se,S)_2$ thin films", *Solar Energy Mater. Solar Cells*, 50 (1998) 31-36.

[8] L.I. Soliman and T.A. Hendia, "Influence of γ-irradiation on the optical and electrical properties of $ZnIn_2Se_4$ films", *Rad. Phys. Chem.*, 50(2) (1997) 175-177.

[9] L. Soliman, T. Hendia and H. Zayed, "Effect of Annealing on the Switching Properties of CuInSeTe thin films", *Fizika A (Zagreb)*, 16(1) (2007) 39-46.

[10] J.Y.W. Seto, "Deposition of Polycrystalline Silicon by Pyrolysis of Silane in Argon", *J. Electrochem. Soc.*, 122(5) (1975) 701-706.

[11] S. Sze and K. Kwok, **"Physics of Semiconductor Devices"**, 3rd ed., John Wiley & Sons, Inc. Hoboken (NJ, 2007).

IRAQI JOURNAL OF APPLIED PHYSICS LETTERS
EDITORIAL BOARD

COPYRIGHT RELEASE FORM

IRAQI JOURNAL OF
APPLIED PHYSICS LETTERS (IJAPLett)

We, the undersigned, the author/authors of the article titled

……
……
……
……
……
……
……

that is submitted to the Iraqi Journal of Applied Physics Letters (IJAPLett) for publication, declare that we have neither taken part or full text from any published work by others, nor presented or published it elsewhere in any other journal. We also declare transferring copyrights and conduct of this article to the Iraqi Journal of Applied Physics Letters (IJAPLett) after accepting it for publication.

The authors will keep the following rights:

1. Possession of the article such as patent rights.
2. Free of charge use of the article or part of it in any future work by the authors such as books and lecture notes after informing IJAP editorial board.
3. Republishing the article for any personal purposes of the authors after taking journal permission.

To be signed by all authors:

Signature:……..date: ……
Printed name: ……

Signature:……..date: ……
Printed name: ……

Signature:……..date: ……
Printed name: ……

Correspondence author:……...
……
Address:……
……
Telephone:……..……..email: ……

Note: Complete and sign this form and mail it to the below address with your finally revised manuscript

The Iraqi Journal of Applied Physics Letters
P. O. Box 88052, Baghdad 12631, IRAQ
www.iraqiphysicsjournal.com
Email: editor@iraqiphysicsjournal.com
Email: editor_ijap@yahoo.co.uk
Email: ijaplett.editor@gmail.com

IRAQI JOURNAL OF APPLIED PHYSICS LETTERS
Volume (6) Issue (1) January-March 2023

CONTENTS